On the Morphology and Stability of Au Nanoparticles on TiO 2 (110) Prepared from Micelle-Stabilized Precursors

ARTICLE *in* LANGMUIR · SEPTEMBER 2006

Impact Factor: 4.46 · DOI: 10.1021/la0610102 · Source: PubMed

8 AUTHORS, INCLUDING:

Joachim Bansmann
Universität Ulm
113 PUBLICATIONS **1,909** CITATIONS

SEE PROFILE

On the Morphology and Stability of Au Nanoparticles on TiO_2(110) Prepared from Micelle-Stabilized Precursors

Stefan Kielbassa,† Annette Häbich,† Johannes Schnaidt,† Joachim Bansmann,† Frank Weigl,‡ Hans-Gerd Boyen,‡ Paul Ziemann,‡ and R. Jürgen Behm*,†

Department of Surface Chemistry and Catalysis, University of Ulm, D-89069 Ulm, Germany, and Department of Solid State Physics, University of Ulm, D-89069 Ulm, Germany

Received April 13, 2006. In Final Form: June 13, 2006

The morphology and stability of well-ordered, nanostructured Au/TiO_2(110) surfaces, prepared by deposition of Au loaded micelles on TiO_2(110) substrates and subsequent oxidative removal of the polymer shell in an oxygen plasma, was investigated by noncontact AFM, SEM and XPS. The resulting arrays of Au nanoparticles (particle sizes 1−5 nm) form a nearly hexagonal pattern with well-defined interparticle distances and a narrow particle size distribution. Particle size and particle separation can be controlled independently by varying the Au loading and the block-copolymers in the micelle shell. The oxygen plasma treatment does not affect the size and distance of the Au nanoparticles; the latter are fully metallic after subsequent UHV annealing (400 °C). The particles are stable under typical CO oxidation reaction conditions, up to at least 200°C, making these surfaces ideally suited as defined model systems for catalytic studies. Significant changes in the height distributions of the Au nanoparticles are found upon 400 °C annealing in O_2. For adlayers with small interparticle distances, this leads to a bimodal particle size distribution, which together with the preservation of the lateral order points to Ostwald ripening.

Introduction

Metal nanoparticles on planar surfaces with a narrow distribution and well-defined interparticle distances in regular, ordered arrays are highly interesting model systems in various fields of fundamental research such as magnetic nanostructures, nanoelectronic devices, heterogeneous catalysis and optical applications. In heterogeneous catalysis, where the size of the reactive particles in supported catalysts is known to play an important and often decisive role for the activity and selectivity of the catalyst,[1] model systems with defined particle sizes and narrow size distributions have been highly useful for studying particle size effects under well-defined conditions.[2] Also, the support has been proposed to directly contribute to the catalytic reaction, e.g., via (reverse) spill-over of reactants.[3−5] In these cases, the density of the deposited nanoparticles on the support will also play an important role. For studies of the transport and surface diffusion processes contributing to the reaction, the possibility to (i) create model systems with defined interparticle separations or even well-ordered arrays of deposited nanoparticles and (ii) vary the interparticle spacing without affecting the particle size or vice versa would be highly useful.

So far, various approaches have been applied to produce model systems with well-defined particle sizes and particle−particle separations with different degrees of perfectness. The most common procedure for deposition of supported metal nanoparticles, physical vapor deposition, results in nanoparticles with a rather broad distribution of particle sizes and interparticle separations.[6] A different approach, which was also applied in the present study, involves the deposition of preformed metal nanoparticles such as tenside- or ligand-stabilized metal clusters[7] or nanoparticles[8] or of metal salt loaded micelles.[6,9] It has been shown for some model cases that reasonably well-ordered adlayers can be obtained this way.[6,9] Crucial steps in these deposition processes are the removal of the organic stabilizer shell, which is required for many applications, and the formation of reduced metal particles when using metal salt loaded micelles as precursors. Well-ordered particle arrangements are also obtained by lithographic techniques such as electron beam lithography[10] or colloidal lithography.[11] The resulting particle sizes of 20−100 nm and the correspondingly large particle separations make these techniques, however, less suitable for catalytic applications.

In the present paper, we report on the formation, structure/morphology, and thermochemical stability, under inert conditions and in a reactive atmosphere, of planar Au/TiO_2(110) model catalysts, which have been prepared by deposition of Au salt loaded block-copolymer micelles[6,9] on atomically flat, fully oxidized TiO_2(110) substrates. After removal of the polymer shell in an oxygen plasma, the Au particles have a desired size (1−5 nm) and well-defined interparticle distances (20−100 nm). The structural characterization was carried out using noncontact atomic force microscopy (nc-AFM) under ultrahigh vacuum (UHV) conditions and by scanning electron microscopy (SEM); the electronic structure and the chemical state of the substrate and the nanoparticle surface were characterized by X-ray

* To whom correspondence should be addressed. E-mail: juergen.behm@uni-ulm.de.

† Department Surface Chemistry and Catalysis.

‡ Department of Solid State Physics.

(1) Sinfelt, J. H. *Surf. Sci.* **2002**, *500*, 923.

(2) Valden, M.; Lai, D.; Goodman, D. W. *Science* **1998**, *281*, 1647.

(3) Conner, W. C., Jr.; Pajonk, G. M.; Teichner, S. J. *Adv. Catal.* **1996**, *34*, 1.

(4) Pajonk, G. M. *Handbook of Heterogeneous Catalysis*; VCH−Wiley: Weinheim, Germany, 1997; pp 1064−1077.

(5) Leppelt, R.; Schumacher, B.; Plzak, V.; Kinne, M.; Behm, R. J. To be published.

(6) Kästle, G.; Boyen, H.-G.; Weigl, F.; Lengl, G.; Herzog, Th.; Ziemann, P.; Riethmüller, S.; Meyer, O.; Hartmann, C.; Spatz, J.; Möller, M. M.; Ozawa, M.; Banhart, F.; Garnier, G.; Oelhafen, P. *Adv. Funct. Mater.* **2003**, *13*, 853. Kästle, G.; Boyen, H.-G.; Weigl, F.; Ziemann, P.; Riethmüller, S.; Hartmann, C.; Spatz, J.; Möller, M. M.; Garnier, G.; Oelhafen, P. *Phase Transitions* **2003**, *76*, 307.

(7) Schmid, G. *Inorg. Synth.* **1990**, *7*, 214.

(8) Bönnemann, H.; Brijoux, W.; Brinkmann, R.; Fretzen, R.; Joussen, T.; Köppler, R.; Korall, B.; Neiteler, P.; Richter, J. *J. Mol. Catal.* **1994**, *86*, 129.

(9) Spatz, J. P.; Mößmer, S.; Hartmann, C.; Möller, M.; Herzog, T.; Krieger, M.; Boyen, H.-G.; Ziemann, P.; Kabius, B. *Langmuir* **2000**, *16*, 407.

(10) Gunter, P. L. J.; Niemantsverdriet, J. W.; Ribeiro, F. H.; Somorjai, G. A. *Catal. Rev. Sci. Eng.* **1997**, *39*, 77.

(11) Werdinius, C.; Oesterlund, L.; Kasemo, B. *Langmuir* **2003**, *19*, 458.

10.1021/la0610102 CCC: $33.50
Published on Web 08/01/2006

photoelectron spectroscopy (XPS). This work is part of a study aimed at the detailed understanding of surface transport processes in catalytic reactions in general and specifically during CO oxidation on Au/TiO_2 catalysts. Consequences of the particles size and particle distances on the catalytic activity of these model catalysts are currently being investigated and will be reported later. We will also compare the present results with previous data on the stability of Au nanoparticles of similar size, which had been produced by physical vapor deposition on similar TiO_2-(110) substrates.[12]

Metal oxide supported Au catalysts have attracted considerable interest over the past decade mainly due of their high catalytic activity at low-temperature oxidation and hydrogenation reactions.[13−15] Despite numerous studies, including various studies on planar model catalysts,[2,12,16−27] important details of the reaction mechanism have not yet been resolved. In particular, the origin and nature of the considerable particle size effects reported in some studies[2,28] are still under debate. These previous studies on Au/TiO_2 model catalysts, however, involved Au nanoparticles created by thermal evaporation of Au under UHV conditions onto an oxide surface (either a bulk oxide surface or a thin oxide film on a single-crystalline metal substrate), with relatively broad distributions in particle sizes and interparticle separations, which are not well-suited for detailed studies of particle size effects and even less for unraveling contributions from transport effects as described above.

Experimental Section

The experiments were performed in a UHV system equipped with a home-built AFM which includes a laser-beam deflection system (maximum scan range: $1\ \mu m \times 1\ \mu m$)[29] and facilities for sample preparation and characterization such as X-ray photoelectron spectroscopy XPS (Specs EA 200), an argon ion sputter gun for sample cleaning, and a thermal evaporation source for in situ metal deposition. An additional high-pressure cell attached to the UHV chamber via a gate valve allowed in situ sample processing up to atmospheric pressure and to introduce samples via a load lock system. Sample heating was performed by a tungsten filament in the UHV chamber and in the high-pressure cell by a boron nitride ceramic heater. The sample temperature was determined via IR-pyrometer (Infraterm IP140, Impac Infrared GmbH, Germany).

To avoid displacement of the Au nanoparticles by the AFM tip, the AFM measurements were performed in the attractive noncontact mode (nc mode). Using this mode, no effect on the Au particle distribution could be detected. X-ray photoelectron spectra were recorded in normal emission using Al Kα radiation, with pass energies of 197.7 eV for overview scans and 29.3 eV for detailed scans, respectively.

Table 1. Overview on the Block-Copolymers, Gold Loadings, and Resulting Mean Particle Heights Used for the Different $Au/TiO_2(110)$ Samples

figure	polymer	Au loading	mean particle height /nm	particle density /cm^{-2}
4a	PS*(312)*-*b*-P2VP*(74)*	0.1	1.5	1.02×10^{11}
3/4b	PS*(312)*-*b*-P2VP*(74)*	0.3	2.9	1.08×10^{11}
4c/5a	PS*(312)*-*b*-P2VP*(74)*	0.5	4.0	1.04×10^{11}
5b	PS*(528)*-*b*-P2VP*(177)*	0.25	4.5	2.10×10^{11}
5c	PS*(1779)*-*b*-P2VP*(857)*	0.025	4.5	1.35×10^{10}

Rutile $TiO_2(110)$ substrates (TBL Kelpin, Germany, one side polished, tolerance of the surface orientation <0.5°) were cleaned by dipping in acetone (5 min in a supersonic bath), in a H_2O_2/H_2SO_4 mixture (1:1) for 10 min and then in Millipore water. Afterward, the samples were calcined in air for 1−2 h in an oven at 950 °C and then cooled in air. This treatment leads to fully oxidized flat sample surfaces with broad terraces (50−200 nm), separated by monatomic steps.[12] The deposition of gold on the freshly cleaned substrates was performed by a micellar technique, which had been applied before for deposition of Au loaded micelles on different substrates, such as Si/SiO_2, Al_2O_3, and $SrTiO_3$ (for details, see refs 6 and 9). In short, a polystyrene (PS)-*block*-poly(2-vinylpyridine) (P2VP) copolymer is dissolved in toluene, where it forms spherical reverse micelles, with the hydrophilic P2VP forming the core and the hydrophobic PS the outer shell. The notation PS(*x*)-*b*-P2VP(*y*) refers to the number of monomers *x* and *y* of the respective polymers. Next, $HAuCl_4$ is added to the solution, which is accumulated in the core of the micelles. Finally, in equilibrium, all micelles are loaded with an equal amount of metal salt. The resulting Au loading is given in Table 1 as Au atoms divided by the total number of P2VP monomers in the solution. The transfer of the Au loaded micelles onto the substrates is carried out by dipping the sample vertically into the solution and removing it at a constant velocity (14 mm min^{-1}). This procedure results in a close-packed, ordered monolayer of the micelles with an intact polymer shell on the substrate (for details of the preparation, see Table 1), where the interparticle distance is determined by the length of the polymer shell. As a final step, the surrounding polymer is removed in an oxygen-plasma (RF−Plasma frequency: 13,56 MHz, P = 50 W, $p(O_2) = 4 \times 10^{-2}$ mbar, time: 20 min, room temperature), which was shown before by TEM measurements to result in bare Au particles on the substrate.[12] Note, that time and temperature have been changed from the usual settings (200 °C, 30 min) in order to obtain better results (see below). After the plasma treatment and transport through air, the samples are introduced into the UHV chamber and first annealed in UHV at 400 °C for 5 min. This procedure, which was tested to have no influence on the order and the height of the Au nanoparticles (see below), was carried out in order to remove adsorbates such as water molecules, which might have been picked up during the transport of the samples in air, and to fully reduce the Au nanoparticles.

Results and Discussion

Surface Composition after Preparation and UHV Annealing. The chemical composition of the resulting model catalyst, after the UHV annealing step, was first characterized by XPS. Figure 1 shows a representative XP spectrum of a $Au/TiO_2(110)$ sample after this first annealing step. Within the sensitivity of these measurements, the sample is free from polymer residues as well as from other contaminants such as chlorine, which could result from the Au salt. Furthermore, only titanium in the Ti^{4+} oxidation state can be detected on the substrate surface (see inset in Figure 1), which is a clear indication for a well-oxidized sample. A simple simulation of a Ti(2p) spectrum using Ti^{4+} and Ti^{3+}-(2p) peaks at 459.2 and 457.2 eV,[30] respectively, shows that less

(12) Kielbassa, S.; Kinne, M.; Behm, R. J. *J. Phys. Chem. B* **2004**, *108*, 19184.
(13) Haruta, M.; Tsubota, S.; Kobayashi, T.; Kageyama, H.; Genet, M. J.; Delmon, B. *J. Catal.* **1993**, *144*, 175.
(14) Haruta, M. *Catal. Surv. Jpn.* **1997**, *1*, 61.
(15) Haruta, M. *Gold Bull.* **2004**, *37*, 27.
(16) Zhang, L.; Persaud, R.; Madey, T. E. *Phys. Rev. B* **1997**, *56*, 10549.
(17) Liu, Z. M.; Vannice, M. A. *Catal. Lett.* **1997**, *43*, 51.
(18) Valden, M.; Pak, S.; Lai, X.; Goodman, D. W. *Catal. Lett.* **1998**, *56*, 7.
(19) Parker, S. C.; Grant, A. W.; Bondzie, V. A.; Campbell, C. T. *Surf. Sci.* **1999**, *441*, 10.
(20) Lai, X.; Goodman, D. W. *J. Mol. Catal. A* **2000**, *162*, 33.
(21) Cosandey, F.; Madey, T. E. *Surf. Rev. Lett.* **2001**, *8*, 73.
(22) Sykes, E. C.; Tikhov, M. S.; Lambert, R. M. *Catal. Lett.* **2002**, *82*, 169.
(23) Lee, S.; Fan, C.; Wu, T.; Anderson, S. L. *Surf. Sci.* **2005**, *578*, 5.
(24) Choudhary, T. V.; Goodman, D. W. *Appl. Catal. A* **2006**, *291*, 32.
(25) Starr, D. E.; Shaikhutdinov, S. K.; Freund, H.-J. *Top. Catal.* **2005**, *36*, 33.
(26) Zhao, Z.; Diemant, T.; Häring, T.; Rauscher, H.; Behm, R. J. *Rev. Sci. Instrum.* **2005**, *76*, 123903.
(27) Diemant, T.; Schumacher, B.; Leppelt, R.; Zhao, Z.; Rauscher, H.; Behm, R. J. To be published.
(28) Bamwenda, G. R.; Tsubota, S.; Nakamura, T.; Haruta, M. *Catal. Lett.* **1997**, *44*, 83.
(29) Wiechers, J. Ph.D. Thesis; Ludwig-Maximilian-Universität: München, 1993.
(30) Gonbeau, D.; Guimon, C.; Pfister-Guillouzo, G.; Levasseur, A.; Meunier, G.; Dormoy, R. *Surf. Sci.* **1991**, *254*, 81.

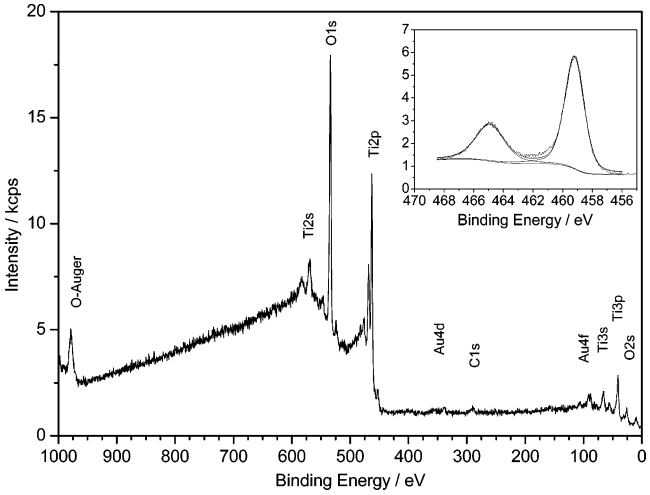

Figure 1. Wide range XP spectrum of a typical TiO_2(110) sample covered with Au loaded micelles after deposition, oxygen plasma treatment, and UHV annealing (400 °C, 5 min). Inset: Detail spectrum of the Ti(2p) region after the same treatment.

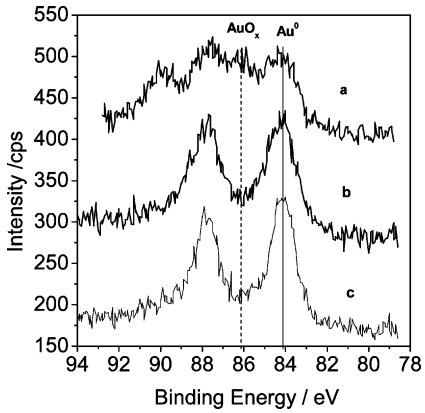

Figure 2. Detail XP spectra of the Au(4f) region of a Au/TiO_2(110) sample (a) directly after preparation, (b) after annealing in UHV for 5 min, and (c) after annealing in 20 mbar O_2 at 400 °C for 30 min.

than 3% Ti^{3+} in the surface region could easily be detected in the spectrum at the present resolution. Thus, the chemical state of the TiO_2 substrate used here is comparable to that of the support of powder catalysts. It should be noted that the commonly applied pretreatment of single-crystal TiO_2 samples, including annealing in UHV to high temperatures and Ar^+ sputtering (which is often applied also in order to enhance the conductivity of the samples), leads to a different result in XPS. In these cases, one obtains a partly reduced surface region, especially after annealing in UHV at higher temperatures for obtaining flat surfaces.[2,16,31] In addition to a modified electronic structure of the substrate, the partial reduction of the surface may result in a different chemical behavior upon interaction with reactive gases such as O_2. Several groups even reported a segregation of titanium to the surface, in combination with a pronounced modification of the substrate.[31,32]

The subsequent initial annealing procedure in UHV also serves to fully reduce the Au nanoparticles on the surface. Directly after the oxygen plasma treatment, the Au surface is usually highly oxidized, which is indicated by a broad and less structured peak for the Au(4f) doublet with contributions from both Au^0 and Au^{n+} species (Figure 2, curve a). After annealing in UHV, the Au oxides are decomposed, resulting in the exclusive observation

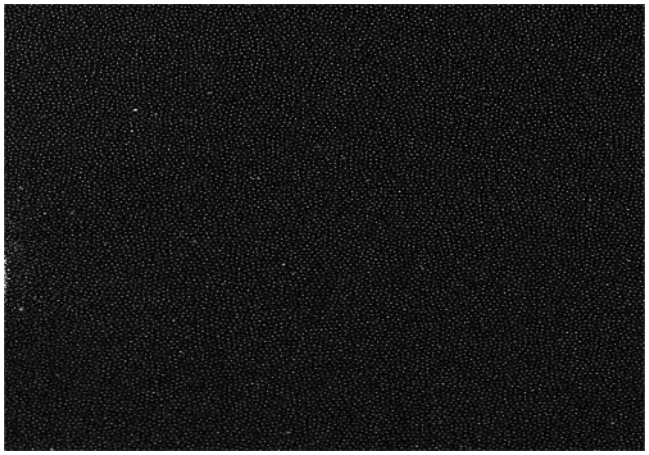

Figure 3. SEM image (3.1 μm × 2.1 μm) of the Au/TiO_2(110) surface after oxygen plasma treatment (Au loading 0.3, P*S(312)-b*-P2vP*(74)*, particle height 2.9 nm, see Figure 4b).

of metallic Au^0 species, with a sharp Au($4f_{7/2}$) peak at 84.0 eV (Figure 2, curve b). This binding energy agrees well with previous reports on bulk Au and larger Au nanoparticles.[16] Further details on the composition of the Au oxides formed by the oxygen plasma treatment and the decomposition of the gold oxides during UHV annealing can be found in ref 6. AFM images accessible as supporting material show that the order and height of the Au particles is not significantly changed by this annealing step.

Variation of Particle Sizes and Distances. Before coming to the main point of this section, the variation of the particle size and distance by varying the Au loading of the micelles and the polymer shell, we briefly comment on the pretreatment necessary for removal of the polymer shell and the subsequent reduction of the resulting oxidized particle surface. In the oxygen plasma treatment, we found a strong effect of the substrate temperature on the particle heights on TiO_2, in contrast to previous observations on other substrates such as Al_2O_3, Si/SiO_2, $SrTiO_3$, or diamond.[6,9,33] If the substrate temperature during this treatment is kept at 200 °C, the mean particle height changed significantly on TiO_2(110), whereas for Au/Al_2O_3 or Au/SiO_2 (for AFM images, see the Supporting Information), this is not the case, even though similar type micelles were used and deposited in the same way. In fact, on TiO_2(110), a large part of the Au particles has nearly vanished. Consequently, throughout this work, the oxygen plasma treatment was performed with the substrate held at room temperature. The subsequent UHV annealing at 400 °C had no significant effect on the particle heights and distribution.

The very homogeneous structure of the arrays of nanoparticles resulting from the micelle deposition technique is illustrated in the large-scale SEM image in Figure 3 (3.1 μm × 2.1 μm). It shows a surface covered with Au nanoparticles, which are identical to the particles depicted in the AFM image in Figure 4b (particle height 2.9 nm, Au loading see Table 1). Over the entire area imaged, we find a completely homogeneous pattern of particles, with essentially no defects, contaminations, or other irregularities.

Subsequently, we first investigated the deposition of micelles with varying Au loading, but identical polymer spacer, which results in an average spacing between Au particles of 25 nm. More detailed information on the micelles, their gold loadings, and the resulting particle sizes can be found in Table 1. Representative large-scale (Figure 4, left, 800 nm × 800 nm) and

(31) Diebold, U. *Surf. Sci. Rep.* **2003**, *48*, 53.
(32) Kolmakov, A.; Goodman, D. W. *Catal. Lett.* **2000**, *70*, 93.
(33) Boyen, H.-G.; Kästle, G.; Weigl, F.; Koslowski, B.; Dietrich, C.; Ziemann, P.; Spatz, J. P.; Riethmüller, S.; Hartmann, C.; Möller, M.; Schmid, G.; Garnier, M. G.; Oelhafen, P. *Science* **2002**, *297*, 1533.

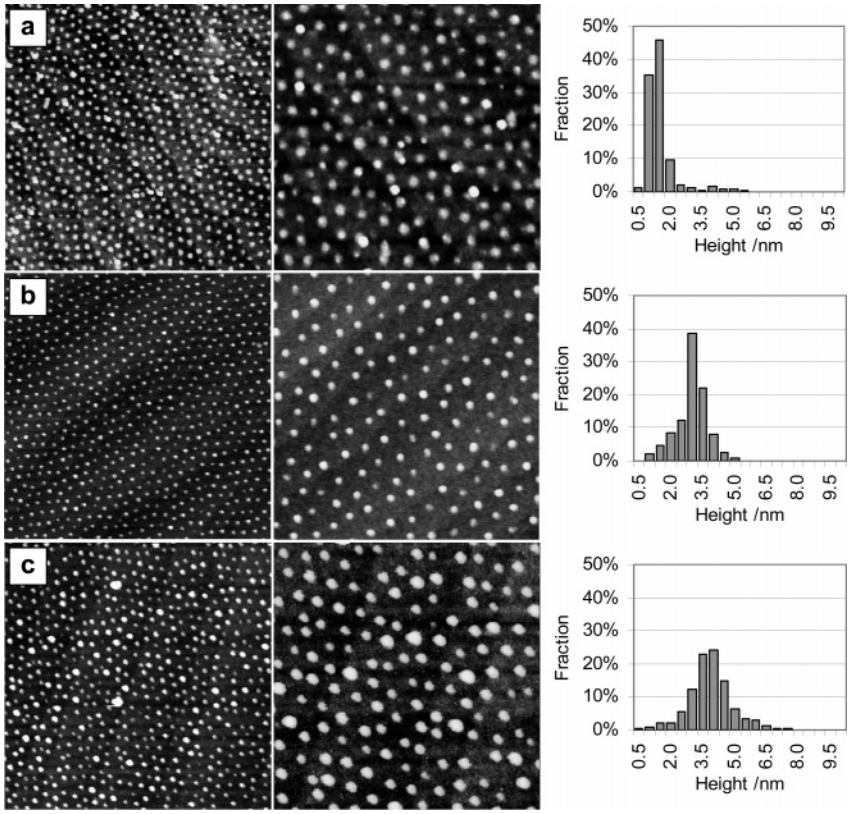

Figure 4. nc-AFM images (left and middle column) and corresponding height distributions (right column) of micelle-based Au particles of different sizes on TiO_2(110) (preparation see text and Table 1). The mean heights correspond to (a) 1.5, (b) 2.9, and (c) 4.0 nm. The interparticle distance was 25 nm. Image sizes: 800 nm × 800 nm in the left column and 400 nm × 400 nm in the center column.

medium-scale (Figure 4, middle, 400 nm × 400 nm) nc-AFM images illustrate the geometric order obtained for the three different Au loadings. In all cases, the particle density is around $(1.05 \pm 0.05) \times 10^{11}$ cm^{-2}. The images clearly demonstrate a highly organized structure with a nearly hexagonal symmetry.

Since the measured diameter of the particles is strongly affected by the actual shape of the AFM tip and may not give the actual size, we mainly evaluated the particle heights which are measured precisely. For the determination of the height distribution, at least three different areas on the surface with about 350−700 particles have been evaluated. The resulting particle size distributions are depicted in the right column of Figure 4. The mean particle heights were determined to be 1.5 (a), 2.9 (b), and 4.0 nm (c). The variation of the particle heights is mainly attributed to statistical variations in the metal salt loading of the individual Au micelles. The dispersion becomes broader with increasing mean particle sizes. Although for the smallest particles over 80% can be found between the narrow range of 1.0 and 1.5 nm, the variation is higher for the bigger particles. However, when scaling the half width of the height distribution to the mean height, this value is nearly independent of the absolute height regime.

The results of controlled variation of the interparticle distances, by varying the length of the polymer, is illustrated in the nc-AFM images in Figure 5, where the interparticle distance rises from ∼25 nm (cf. Figure 5a) via ∼60 nm (Figure 5b) to ∼100 nm (Figure 5c). Accordingly, the particle density changes from 1.05×10^{11} cm^{-2} via 2.1×10^{10} cm^{-2} to 1.35×10^{10} cm^{-2} (for details on the polymers, see Table 1). Due to the higher amount of P2VP monomers in the longer polymer chains, the corresponding Au loading (which is given as Au−atoms/P2VP monomers) had to be reduced from 0.5 to 0.25 and 0.025 in order to get particles of similar size. Although different polymers and gold loadings have been used, the mean particle height in Figure 5, panels b and c, is around 4.5 nm and therefore comparable to the sample with the small interparticle distance (Figure 5a).

To illustrate the advantage of this method compared to the thermal evaporation of gold concerning the control on the size and interparticle distance, Figure 6 shows the structural order and height distribution of Au particles (coverage: 0.3 ML) prepared by thermal evaporation on an identical substrate. The sample has been postannealed in air to 500 °C in order to obtain particles which have heights and densities comparable to the samples prepared by the micellar technique (see also ref 12). The resulting surface displayed in Figure 6 exhibits a mean particle height of 2.5 nm and a density of 3.1×10^{11} cm^{-2}. However, the interparticle distances are much less homogeneous; some particles seem to agglomerate, whereas others have larger distances between each other. In addition, the height distribution of these particles is much broader than those obtained by micellar deposition. Only about 50% of the particles are in the range of 2.5 ± 0.5 nm, whereas typical 70% of the particles prepared by the micellar technique can be found in the regime of 3.0 ± 0.5 nm at a mean height of 2.9 nm. Moreover, particles with heights down to 0.5 nm can only be found on the sample prepared by evaporation.

Stability in CO/O_2. To detect changes in the morphology of the Au particles on the TiO_2 sample upon exposure to a reactive CO/O_2 mixture during typical reaction temperatures, we analyzed the particle size distribution after different annealing times in 1:4 CO/O_2 mixtures (50 mbar total pressure, 80 °C annealing temperature). These parameters correspond to typical reaction conditions for Au/TiO_2 powder catalysts.[34] For the investigations

(34) Schumacher, B.; Plzak, V.; Kinne, M.; Behm, R. J. *Catal. Lett.* **2003**, *89*, 109.

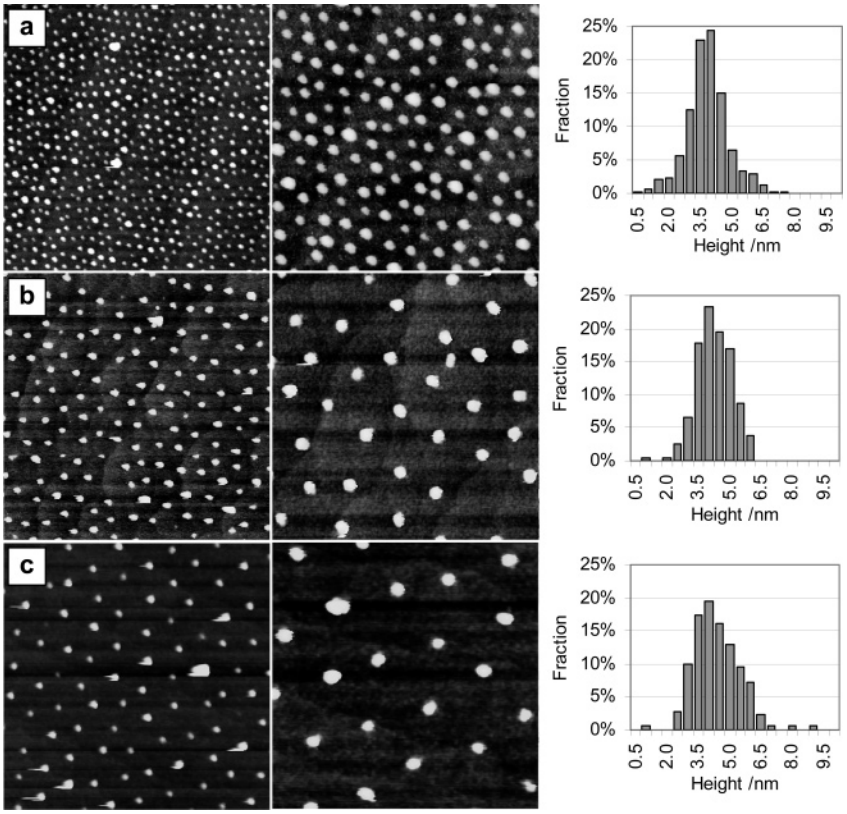

Figure 5. nc-AFM images (left and middle column) and corresponding height distributions (right column) of micelle-based Au particles on TiO_2(110) with different interparticle distances, using micelles with different block copolymers (preparation see text and Table 1). The mean height corresponds to 4.0−4.5 nm, the mean interparticle distances are (a) 25, (b) 60, and (c) 100 nm. Image sizes: 800 nm × 800 nm in the left column and 400 nm × 400 nm in the center column.

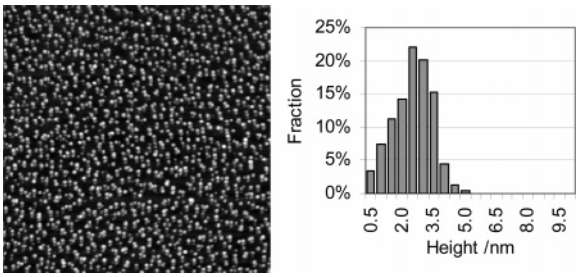

Figure 6. nc-AFM image (800 nm × 800 nm) and corresponding particle height distribution of a Au/TiO_2(110) surface prepared by Au evaporation (coverage: 0.3 ML) and subsequent annealing to 500 °C in air for 30 min.

shown here, the same sample was examined after several time intervals (30 min, 1 h, 13 h, and 60 h) in this reaction mixture. This treatment did not lead to any significant changes in the surface and particle morphology. Finally, the sample was annealed for 13 h in this reaction mixture at 200°C. In AFM images reproduced in Figure 7, we compare the surface of the sample before and after the complete stability test. Although the temperature during the last treatment was significantly higher than the temperature typically applied during CO oxidation on powder catalysts (80°C), we could not identify any significant changes on the particle morphology. Clearly, these Au particles are stable under reaction conditions even for a long time period. This result is in good agreement with our previous findings on Au/TiO_2 samples prepared by evaporation, where we equally observed negligible changes after 80 °C annealing in a CO/O_2 mixture.

Comparable studies have been carried out by Goodman and co-workers on evaporation-produced Au/TiO_2(110) samples. These authors reported significant particle growth already after exposing the sample to ∼10 mbar of a 1:1 CO/O_2 mixture at room temperature, which they mainly attributed to the presence of O_2.[2,20] Similar observations were made at 180 °C exposure.[35] These structural changes were proposed as the origin for the observed decay of the catalytic activity by up to 1 order of magnitude during 2 h reaction time.[20] On the other hand, this finding is not consistent with results on Au/TiO_2 powder catalysts, where Au particle growth under CO reaction conditions (80°C) was found to be small[36] or even absent.[34] The discrepancy between these results may be due to the different state of the substrate (fully oxidized or partly reduced). In previous work, we found indeed, that the substrate pretreatment influences the Au particle stability on TiO_2(110) surfaces during O_2 treatment at room temperature.[12] The results presented in this paper demonstrate that the samples prepared by the micelle technique show a high particle stability, which is comparable to that of powder catalysts. Differences compared to evaporation-produced Au/TiO_2(110) samples may be related to the more spherical shape of the micelle-based Au nanoparticles, compared to the flatter shape of small particles created by evaporation. These characteristics make the micelle based surfaces well suited for application as model catalysts.

Temperature Stability in O_2. The stability of the Au particles in O_2 at elevated temperatures is a further important point to be considered for Au/TiO_2 model studies, since the preparation of realistic dispersed Au/TiO_2 catalysts often involves a calcination step, typically at 400 °C. In previous experiments on evaporated gold particle based model systems, we found a strong change of the particle size after annealing in O_2 at 400 °C for 30 min.[12]

(35) Kolmakov, A.; Goodman, D. W. *Surf. Sci.* **2001**, *490*, L597.
(36) Konova, P.; Naydenov, A.; Venkov, Cv.; Mehandjiev, D.; Andreeva, D.; Tabakova, T. *J. Mol. Catal. A* **2004**, *213*, 235.

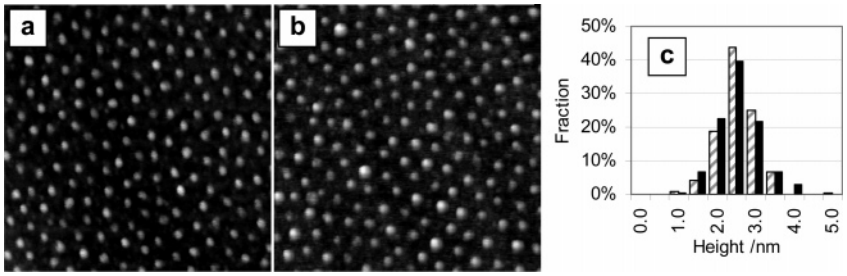

Figure 7. nc-AFM images (a,b) and corresponding particle height distribution (c) of 3 nm Au particles (mean interparticle distance: 25 nm) on TiO_2(110): (a) before (hatched bar in c) and (b) after (solid bar in c) annealing for 13 h in 50 mbar CO/O_2 (1:4) at 200 °C.

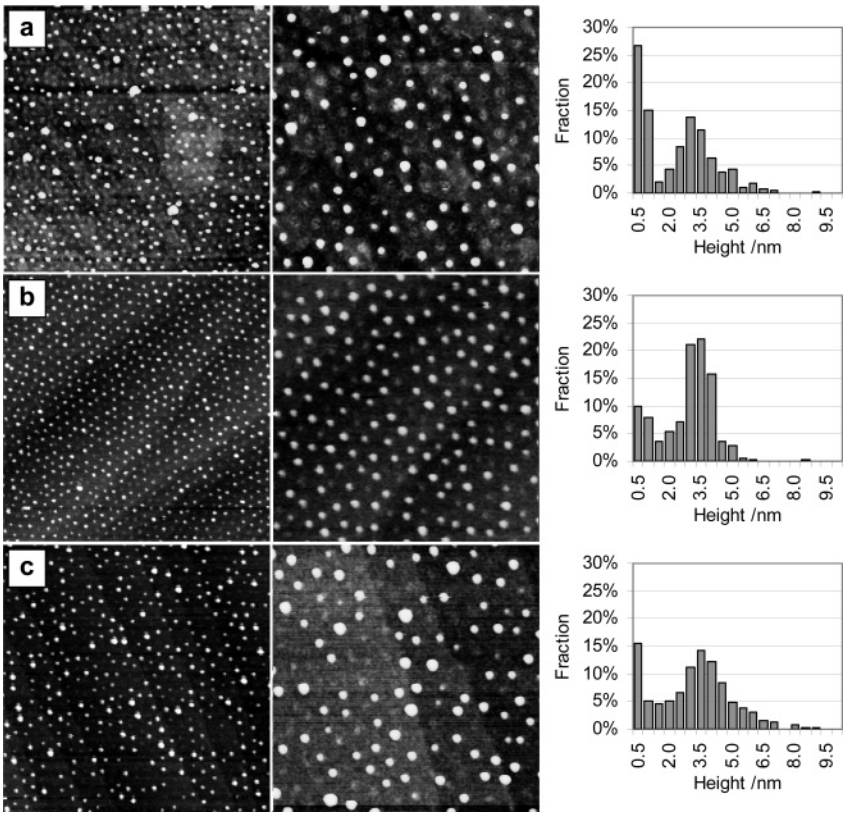

Figure 8. Set of nc-AFM images and particle height distributions of Au/TiO_2(110) samples with different size Au particles (a) 1.5, (b) 2.9, and (c) 4.0 nm, interparticle distance 25 nm) after annealing for 30 min at 400 °C in 20 mbar O_2 (before annealing see Figure 4). Image sizes: 800 nm × 800 nm in the left column and 400 nm × 400 nm in the center column.

In the present study, we examined the stability of micelle-based particles upon annealing in O_2 under similar conditions (30 min, 20 mbar O_2, 400 °C). Based on XPS measurement, the Au particles are still purely metallic; that is, the chemical state is not changed by this treatment. AFM measurements after the O_2 treatment at 400 °C show, however, that the size and size distribution of the Au particles (see Figure 8) have significantly changed compared to those before annealing (cf. Figure 4). The heights of the particles are different for all samples, with significant amounts of very small particles (sizes <1 nm), whereas on the other hand, larger particles than before annealing are found as well. Thus, the height distributions resemble a bimodal statistical model. This result is clearly different from our findings after UHV annealing at 400 °C or annealing in CO/O_2 at 200 °C. In contrast to the changes in particle sizes, the ordered arrangement of the particles is still conserved. The latter conclusion was confirmed by large-scale images recorded before and after O_2 annealing (see Figure 9) and the corresponding autocorrelations (Figure 9, insets). Both insets clearly display the conservation of the hexagonal organization of the particles.

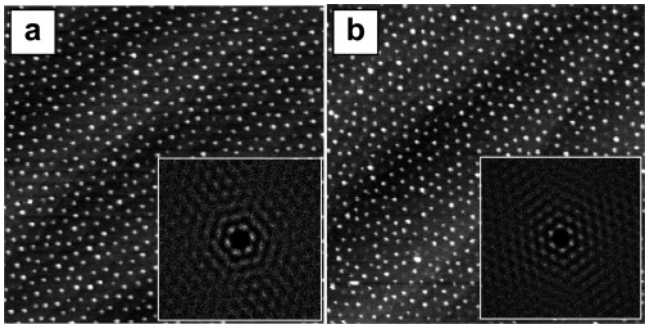

Figure 9. Large-scale AFM images (800 nm × 800 nm) and autocorrelation function (inset) of a Au/TiO_2(110) sample (a) before annealing in O_2 (cf. Figure 4b) and (b) after annealing in O_2 (cf. Figure 7b).

In total, these results are a clear indication for an Ostwald ripening mechanism, operating via detachment and condensation of mobile Au or AuO_x species. For a cluster coalescence mechanism, the

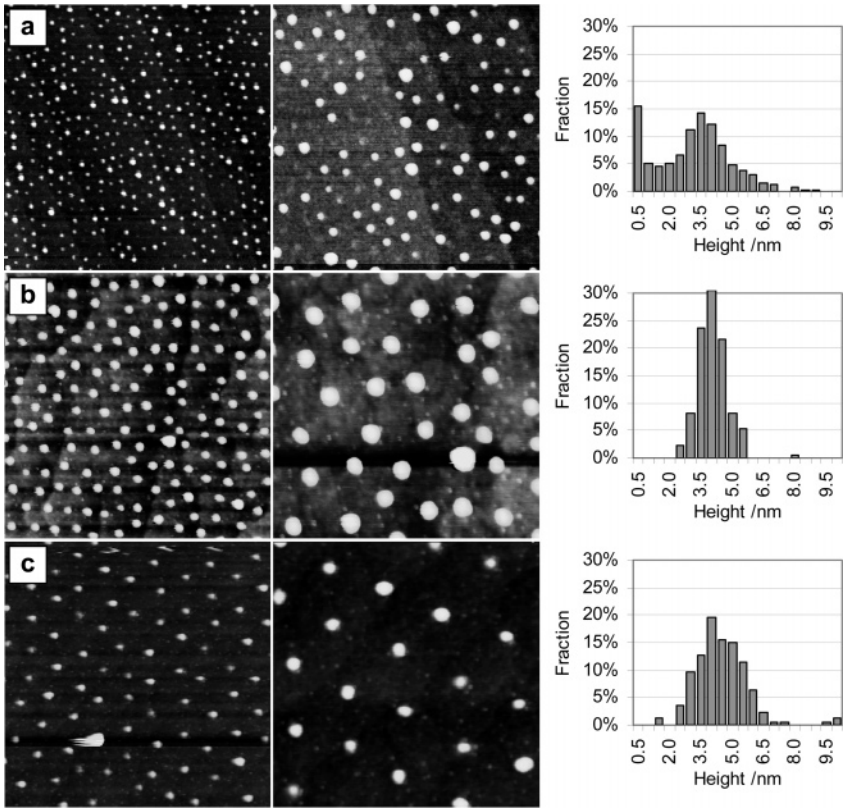

Figure 10. nc-AFM images and particle height distributions of a Au/TiO_2(110) samples with different interparticle distances of (a) 25, (b) 65, and (c) 100 nm after annealing for 30 min at 400 °C in 20 mbar O_2 (before annealing: mean particle height 4 nm, see Figure 5). Image sizes: 800 nm × 800 nm in the left column and 400 nm × 400 nm in the center column.

arrangement of the Au nanoparticles should be much more disordered after O_2 annealing.

Investigations of model catalysts with larger interparticle separations lead to different results for the same treatment, as illustrated in the AFM images and related height distributions shown in Figure 10. The corresponding data before annealing are displayed in Figure 5. Comparison of the height distributions, especially of the maxima of the distribution, shows that the changes induced by the reactive annealing treatment are more pronounced for particles with smaller distances (Figure 10a) than for those with larger distances (Figure 10b,c). For shorter interparticle separations, the mobile Au or AuO_x species detached from the particles are sufficiently mobile to reach the neighboring Au islands and to condense at them. This represents a classic Ostwald ripening mechanism and leads to the formation of a bimodal particle size distribution. For the larger separations, the changes in particle heights are small. Instead, we find additional, much smaller particles between the large particles in Figure 10b,c, which have not been present before annealing. Typically, they are between 0.3 and 1.0 nm high with a maximum at 0.5−0.6 nm. Their particle densities are $\sim 5.0 \times 10^{10}$ cm^{-2} (surface imaged in Figure 10b) and $\sim 2.6 \times 10^{10}$ cm^{-2} (surface imaged in Figure 10c) compared to 2.1×10^{10} and 1.35×10^{10} cm^{-2} for the larger particles. (The small particles were counted extra and not included in the particle height distributions.) These observations can be explained by the same process as described above (surface transport via mobile Au or AuO_x species) during annealing in the O_2 atmosphere, but in this case, the distances are too large for them to always reach the neighboring Au particles, and part of them instead nucleate new Au particles, most likely on substrate defects. The volume V of the newly formed particles with heights around 0.5 nm is very small ($V \cong 0.06$ nm^2, assuming spherical particles) compared to the large particles with heights of ~4.5 nm ($V \cong 46$ nm^2), so that the height of the original particles is not significantly changed during this process.

Comparable results, the absence of Au surface oxides and significant morphological changes, have been reported also in previous studies on bulk Au surfaces,[37] micelle based Au/diamond model systems[33] and Au particles prepared by thermal evaporation on fully oxidized TiO_2 substrates[12] upon 400 °C O_2 annealing. For the latter particles, we found that starting with flat particles ($h = 0.35$ nm) and high particle densities ($\sim 4 \times 10^{12}$ cm^{-2}), annealing in O_2 (400 °C, 50 mbar) results in significant particle growth (~1.3 nm height after reactive annealing) and a decay in particle density by a factor of 6. It is important to note that both factors, the O_2 atmosphere and elevated temperatures, are needed to induce these morphological changes. Neither 400 °C UHV annealing nor room-temperature exposure to O_2 alone results in any significant changes. In contrast, Sykes et al. found rapid sintering of small Au particles already for room-temperature exposure to air,[38] where the authors speculated that the sintering process was supported by the presence of water vapor. On (surface reduced) TiO_2 surfaces prepared by sputter/annealing cycles, exposure to O_2 induces Au particle growth at 180°C [32;35] and even at room temperature.[20]

Based on our present results and data reported previously, the following conclusions can be drawn.

The instability of Au particles on fully oxidized TiO_2(110) substrates in O_2 at elevated temperatures is not restricted to very small particles. We find clear morphological changes even for particle heights up to 4.5 nm.

(37) Koslowski, B.; Boyen, H.-G.; Wilderotter, C.; Kästle, G.; Ziemann, P.; Wahrenberg, R.; Oelhafen, P. *Surf. Sci.* **2001**, *475*, 1.
(38) Sykes, E. C.; Williams, F. J.; Tikhov, M. S.; Lambert, R. M. *J. Phys. Chem. B* **2002**, *106*, 5390.

At smaller interparticle separations (25 nm), which are, however already larger than typical values in highly disperse, realistic Au/TiO_2 catalysts, O_2 treatment leads to particle growth via an Ostwald ripening mechanism, via mobile Au or AuO_x species, rather than via aggregation of mobile Au particles (particle coalescence). This is evidenced by the bimodal particle height distribution and the preservation of the hexagonal arrangement of the particles.

For even larger interparticle separations, the mobility of these species is not sufficient to reach the nearest Au particle, which results in nucleation and growth of additional small Au particles between the initial Au particles.

These findings are important for a further use of these samples as model catalysts. Although calcining at 400 °C is a typical step in Au/TiO_2 powder catalyst preparation,[34] similar treatment of Au model catalysts should be avoided, even for model catalysts with relatively large separations between Au nanoparticles, if the narrow size distributions of these systems shall be maintained. Furthermore, considering the density of Au particles on the TiO_2 support in realistic catalysts, an O_2 induced formation of new Au particles as observed in the low density samples in Figure 10a,b is unlikely, which practically rules out catalyst reactivation by calcination treatments.

Conclusions

We have demonstrated that nanostructured $Au/TiO_2(110)$ surfaces with well-ordered ordered arrays of Au nanoparticles can be produced by deposition of Au-loaded block-copolymer micelles, subsequent oxidative removal of the polymer in an oxygen plasma, and finally brief UHV annealing at 400 °C. This treatment results in a nearly hexagonal pattern of fully metallic Au nanoparticles with well-defined interparticle distances and a narrow size distribution; the polymer is completely removed. By varying the Au loading and the block-copolymers in the micelle shell, particle sizes between 1 and 5 nm have been obtained, interparticle separations varied between 25 and 100 nm. Keeping the sample at RT during the oxygen plasma treatment is crucial to obtain uniform height distributions on $TiO_2(110)$, while temperatures up to 200 °C have no influence on other substrates. The particles are stable in UHV up to 400 °C, comparable to similar size Au nanoparticles on TiO_2-(110) created by evaporation. Significant changes in the morphology and in the height distribution of the Au nanoparticles are found upon annealing the particles in O_2 (400 °C, 20 mbar), which depend strongly on the interparticle distance. At smaller particle distances, we find a bimodal particle size distribution. Together with the preservation of the hexagonal particle pattern, which excludes cluster mobility and therefore cluster aggregation, this points to an Ostwald ripening process, where material transport occurs via mobile Au or AuO_x species. For larger particle distances, however, we observe nucleation of new small particles between the initial Au particles, which is explained by a too low mobility of the mobile species under these conditions to reach neighboring Au nanoparticles, and subsequent nucleation and growth of new particles, possibly on defect sites.

The possibility to independently control and vary the particle size and the interparticle distance and their stability in CO/O_2 reaction atmospheres at realistic pressures and temperatures makes these surfaces ideally suited for model studies on particle size and transport effects in catalytic reactions catalyzed by Au nanoparticles, such as CO oxidation.

Acknowledgment. We thank Prof. P. Walther (ZE Electron Microscopy) for providing access to high resolution SEM imaging. Financial support by the Deutsche Forschungsgemeinschaft via Sonderforschungsbereich 569 and by the Landesstiftung Baden-Württemberg is gratefully acknowledged.

Supporting Information Available: AFM images. This material is available free of charge via the Internet at http://pubs.acs.org.

LA0610102